Pol. J. Environ. Stud. Vol. XX, No. X (XXXX), 1-12
DOI: *10.15244/pjoes/190015* ONLINE PUBLICATION DATE:

Original Research

Pollution and Carbon Sequestration of Highway Runoff in Karst Regions: A Case Study from Guangxi, China

Shan Gao[1], Zhiqin Qing[1], Lang Yang[1], Wenming Feng[1], Shilong Zhu[2, 3], Yincai Xie[2, 3], Fen Huang[2, 3]*

[1]Guangxi Xinfazhan Communication Group Co., Ltd., Nanning 530029, China
[2]Institute of Karst Geology, Chinese Academy of Geological Sciences, Key Laboratory of Karst Dynamics, Ministry of Natural Resources & Guangxi Zhuang Autonomous Region, International Research Centre on Karst, UNESCO, Guilin, Guangxi 541004, China
[3]Pingguo Guangxi, Karst Ecosystem, National Observation and Research Station, Pingguo 531406, Guangxi, China

Received: 29 April 2024
Accepted: 12 June 2024

Abstract

Highway runoff is a known source of pollution; however, its ability to sequester carbon is less well understood. In this study, we examined the pollution, sources, and carbon sequestration of highway runoff in karst areas of Guangxi, China. Runoff samples were collected from different locations during the rainy season. Suspended solids, COD_{Mn}, NH_3–N, and Mn were identified as the primary pollutants. Factor analysis revealed five main sources of highway runoff: traffic, construction, carbonate weathering, rainfall combined with artificial fertilizers, and artificial fertilizers alone. Traffic and carbonate weathering emerged as the predominant factors in the Yaji section of the Guilin Ring Expressway (YJ) and adjacent to the Baizhujing Reservoir (BZJ), while construction and carbonate weather were the primary factors in Xincheng County (XC). The carbon sequestration capacity of highway runoff was the highest in XC, followed by BZJ and YJ. YJ and BZJ accounted for 15-21% of that observed in a karst spring in the same region, revealing a 3.44-4.64–fold increase compared to silicate basins. Thus, despite being a source of pollution, the function of highway runoff as a carbon sink may be key to emission reduction efforts.

Keywords: highway runoff, solute source, factor analysis, carbon sequestration, karst

Introduction

The karst region of the Guangxi Zhuang Autonomous Region (hereafter Guangxi) spans 89,500 km^2 and constitutes 41.57% of the total area of the region [1]. In the 'Guangxi Expressway Network Plan (2018-2030)', the collective expressway length is projected to reach 15,200 km by 2030. Owing to the rapid expansion of expressways, concerns about pollution from surface runoff have increased, particularly with respect to ecologically sensitive water bodies and sources of fresh water.

*e-mail: huangfen@mail.cgs.gov.cn;
Tel.: +8615296002613;
Fax: +86773-5813708.

Suspended solutes (SS), chemical and biochemical oxygen demand (COD and BOD_5, respectively), petroleum derivatives, nutrients (NH_3–N and total phosphorous [TP]), and metals (Pb, Cu, and Zn) have been identified as the dominant components of highway runoff, accounting for 50% of the total load [2, 3]. Their main sources include the leakage of transported goods and abraded particles from tires and road materials [4, 5], while atmospheric deposition and de-icing agents contribute a small amount [2, 6, 7]. Petroleum derivatives primarily originate from fuel and lubricant leakage. Pb and Zn are the principal metals in roadway runoff, with Pb largely originating from vehicular exhaust. The gradual phasing out of Pb additives in gasoline has decreased Pb concentrations in runoff [3, 8]. Zn largely originates from tire and brake lining abrasion [9-11]. Geographic location, pavement materials, regional climate, traffic volume, pavement cleaning, intervals between rainfall events, and rainfall characteristics are also key factors influencing runoff pollution [2-4, 12, 13]. Critically, runoff differs markedly between bridges and road surfaces, with the former causing severe pollution [14].

The impact of highway construction on roadway runoff has received little attention, and the enrichment caused by the weathering of carbonate rocks results in a higher total concentration of heavy metals in the soil [15, 16]. Yet, it is unclear if this results in higher concentrations of heavy metals in highway runoff in karst areas. Carbonate weathering in karst areas sequesters 0.3-0.72 Gt/a of atmospheric and soil-bound CO_2 – 50.5%, 68%, and 2.68 times those of terrestrial vegetation, forests, and shrublands, respectively [17]. Previous studies of karst carbon sinks have largely focused on watersheds [18-20], and carbon sequestration has been attributed to dissolution at the soil–rock interface and bedrock [21] while neglecting surface processes. Local materials are often used for highway construction in karst areas, and road excavation can expose carbonate slopes, the dissolution of which can sequester carbon under hot and rainy conditions [22, 23].

The effect of highway runoff on carbon sequestration in karst regions remains unknown. To address this gap in our knowledge, we collected runoff samples from in-construction and operational highways in the karst areas of Guangxi, China. Samples were collected during the rainy season to measure the concentrations of major ions and heavy metals to understand the pollution status and sources of runoff, as well as its hydrochemical properties and carbon sequestration. Our results provide a basis for remediating pollution, reducing emissions, and enhancing carbon sequestration by highway runoff in karst areas.

Material and Methods

Study Area

A customized collection apparatus was used to obtain 32 runoff samples from multiple locations in the karst areas of Guangxi, including four locations along

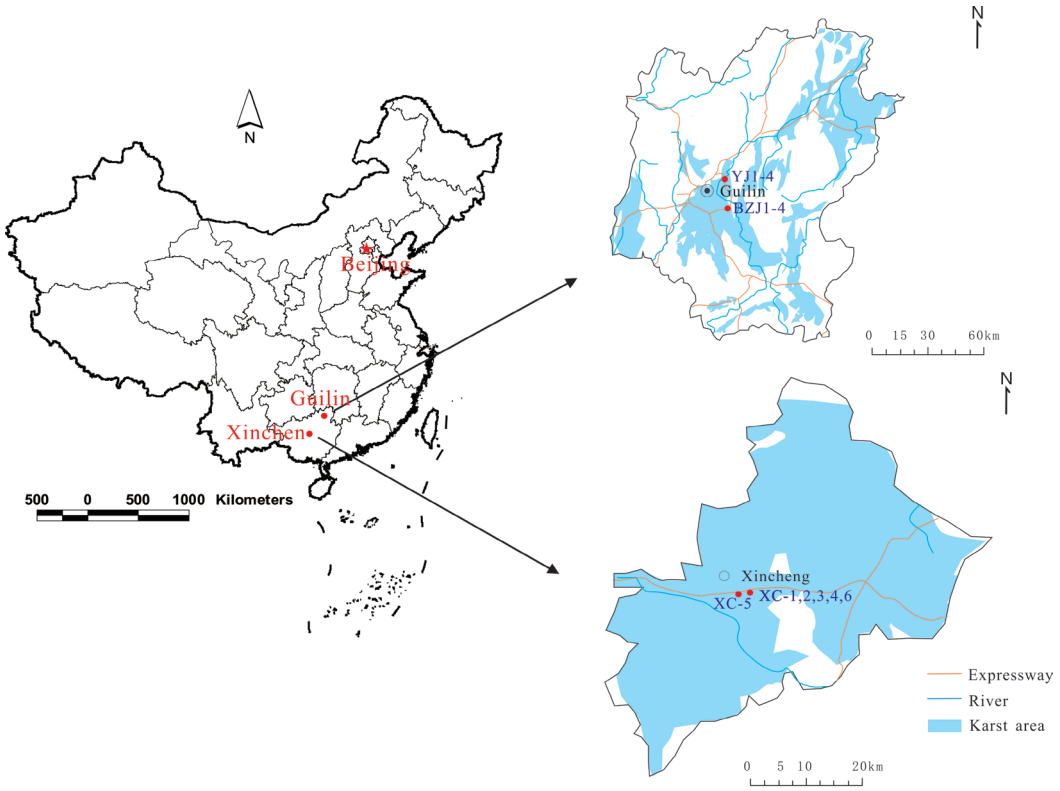

Fig. 1. Map of the sampling sites and hydrogeologic background.

the Yaji (YJ) section of the Guilin Ring Expressway, four adjacent to the Baizhujing Reservoir (BZJ) in Guilin City, and six along the Laidu Expressway in Xincheng County (XC) in Laibin. YJ samples exclusively consisted of road surface runoff, while those from the BZJ and XC (XC-1 and XC-3) were composed of bridge runoff; the remaining samples were of road surface runoff. Sampling was conducted from April-May in Guilin and April-July 2023 in XC, with precipitation of 130 mm and 453 mm, respectively.

The YJ and BZJ areas have a subtropical monsoon climate, with rainfall concentrated from March-June and frequent heavy downpours, resulting in an annual precipitation of 1923 mm. The topography of these areas includes clustered peaks and depressions of Devonian limestone of the Rongxian Formation (D_3r)**.** In contrast, XC is located in a transitional zone, from a subtropical to tropical monsoon climate, and experiences abundant sunlight, a temperate climate, and heavy rainfall. The terrain is marked by erosional hills with subtle undulations and an elevation of 145-180 m a.s.l. and vertical variations of 35 m. Weathered limestone from the Lower Triassic Qixia Formation (P_1q) predominates (Fig. 1). All sampling sites are situated in regions covered by carbonate rocks.

Sampling and Hydrochemical Analyses

A handheld water quality meter (PONSEL Multy 8320, France) was used to measure in situ parameters (e.g., water temperature [T, ºC], pH, and electrical conductivity [EC, µs/cm]) during sample collection. Portable hardness and alkalinity test kits (Merck Germany) were used to titrate in situ Ca^{2+} (mg/L) and HCO_3^- (mmol/L), with accuracies of 0.1 mg/L and 0.01 mmol/L, respectively. Temperature and rainfall were recorded using a self-recording rain gauge (Davis Instruments 6466M, USA). We collected groundwater samples using four 500-mL polyethylene bottles to analyze anions and cations. Three drips of 1:1 HNO_3 were added to samples for cation analysis. An IRIS Intrepid II XSP (Thermo Fisher Scientific, USA) full-spectrum inductively coupled plasma-optical emission spectrometer was employed for cation analysis, and an 883-ion chromatograph (Metrohm 883, USA) was used for anion analysis. Additional analyses were performed using a T6 Nova spectrophotometer (Persee Analytics, USA) and an iCAP Q inductively coupled plasma-mass spectrometer (Thermal Fisher Scientific, USA). The main chemicals tested included K^+, Na^+, Ca^{2+}, Mg^{2+}, Cl^-, SO_4^{2-}, HCO_3^-, NO_3^-, Al, Cu, Pb, Zn, Cr, Ni, Co, Cd, Mn, As, Hg, and Sr.

Data Analysis

Factor Analysis

Factor analysis (FA), as described by Wang et al. [24], was used to condense interrelated variables with complex relationships into composite factors. This approach disentangles the correlations among variables, thereby facilitating their interpretation. We employed R-type FA using SPSS v. 20 (IBM Corp., USA) to identify the primary factors influencing the chemical components of highway runoff.

Calculating Karst Carbon Sinks

The inorganic carbon output derived from the consumption of atmospheric and soil-bound CO_2 through karst processes can be calculated as follows [25]:

$$(Ca_{1-x} \bullet Mg_x)CO_3 + CO_2 + H_2O \rightarrow (1 - x)Ca^{2+} + xMg^{2+} + 2HCO_3^- \quad (1)$$

$$CCSF = 0.5 \times 12 \times (R/d) \times DIC \times 1000 \quad (2)$$

In Equation (2), *CCSF* (kg • C/km^2 d) represents the carbonate weathering carbon-sink flux, where *R* is runoff (m) between two adjacent sampling intervals, *d* is the number of days between two adjacent sampling intervals, and DIC (mmol/L) is the concentration of dissolved inorganic carbon generated by weathering. The molar atomic weight of carbon (12), the ratio of HCO_3^- generated by carbonate weathering derived from the atmosphere (0.5), and 1000 are unit conversion coefficients. We assumed that dissolved carbon could be approximated by bicarbonate alone, [DIC] = [HCO_3^-], which holds for pH ≈ 8 [25]. Given that highway surfaces are impermeable, nearly all runoff is directed toward drainage systems. Hence, measured rainfall was used to approximate runoff volumes.

Results and Discussion

Highway Runoff Quality

Conventional runoff pollutants include SS, COD and BOD, trace metals (primarily Cd, Cr, Cu, Ni, Pb, and Zn), and various N and P species [2], with SS primarily originating from atmospheric deposition, followed by vehicle wear and road abrasion [2, 9, 10]. A reference value for SS was adapted from the 'Water Quality for Landscape Water Use in Urban Sewage Reuse' standard (GB/T 18921-2019) [26] established by the General Administration of Quality Supervision, Inspection, and Quarantine in 2019, which stipulates a threshold of 20 mg/L. Other parameters were compared with the primary and supplementary criteria outlined in the Chinese 'Surface Water Quality Standards for Drinking Water Sources' (GB3838–2002) [27]. The mean concentrations of the chemical constituents in the highway runoff were classified as shown in Table 1, with Standards I–III of centralized domestic drinking water sources and areas and IV–V designated for general

Table 1. Classifications of hydrochemical compounds of highway runoff.

Compound	Unit	Limit	YJ -1	YJ -2	YJ-3	YJ -4	BZJ-1	BZJ-2	BZJ-3	BZJ-4	XC-1	XC-2	XC-3	XC-4	XC-5	XC-6
COD_{Mn}	mg/L		I	III	II	III	II	II	III	IV	II	II	II	II	II	II
SS		20	↑	↑	↑	↑	↑	↑	↑		↑	↑		↑	↑	↑
NH_3–N			I	I	I	III	IV	V	II	III	I	I	III	II	I	I
Cl^-		250														
SO_4^{2-}		250														
NO_3–N		10														
F^-																
Petroleum			I	I	\	III	III	III	III	III	III	III	III	I	III	I
Co		1														
TP	μg/L		II	II	II	III	II	II	II	II	II	II	II	II	II	II
Cu			I	I	I	I	I	I	I	I	I	I	I	I	I	I
Pb			I	I	I	I	III	I	I	I	I	I	I	I	I	I
Zn			I	II	I	II	II	II	II	II	I	I	I	I	I	I
Cr			I	I	I	I	I	I	I	I	I	I	I	I	II	I
Cd			I	I	I	I	I	I	I	I	I	I	I	I	I	I
Mn		100		↑					↑	↑						
As			I	I	I	I	I	I	I	I	I	I	I	I	I	I
Hg			I	I	I	I	I	I	I	I	I	I	I	I	III	I
TFe		300														

Note: ↑ indicates that the compound exceeds a standard limit. Abbreviations: COD, chemical oxygen demand; TFe, total iron; TP, total phosphorous; SS, suspended solutes.

industrial and agricultural water usage and water bodies with typical landscape requirements, respectively.

Table 1 shows that landscape attributes (e.g., SS) surpassed the thresholds in nearly all locations. Nutrient indicators, such as NH_3–N and COD_{Mn}, exceeded the limits at BZJ, whereas Mn exceeded the standards at YJ and BZJ. The constituents of runoff pollution in karst regions mirror those of surface streams. The pH of the runoff ranged from 6-9, aligning with the specifications outlined in GB3838–2002. NH_3–N and TP are primarily from roadside plant fertilization and atmospheric deposition [2], while COD and BOD originate from organic compounds emitted in vehicular exhaust, including petroleum hydrocarbons (PHC) and polycyclic aromatic hydrocarbons (PAHs). Zn, Mn, and Fe are largely derived from tire and brake lining abrasion, with possible contributions from the atmosphere [2, 9-11].

The water quality at all three sampling locations was satisfactory, with no instances of TP, petroleum compounds, or Pb exceeding the regulatory thresholds. The recently operational XC section displayed superior water quality relative to the YJ and BZJ sections, which may be attributed to the accumulation of pollutants from traffic. The water quality of pavement runoff (YJ) was superior to that of bridge runoff (BZJ), consistent with the observations of Smith et al. [28].

Greater deviations from the GB3838-2002 standards, especially for SS and COD, were observed in pavement runoff from the Liuzhen Expressway in Guizhou Province's karst region, where exceedance rates for SS, COD, BOD_5, petroleum compounds, NH_3–N, TP, Pb, and Zn are 96.4%, 98.8%, 84.5%, 100%, 71.8%, 64.7%, 68.3%, and 0%, respectively [29]. In this study, the rates of exceedance for SS, COD, NH_3–N, and Mn were 75%, 16%, 13%, and 13%, respectively, with mean concentrations of 78.33 mg/L, 3.27 mg/L, 0.08 mg/L, and 12.9 µg/L (Fig. 2); all other constituents were within acceptable limits. In contrast, the event mean concentrations (EMCs) of COD, BOD_5, NH_3–N, TN, and TP in the non-karstic area surrounding the Nanjing Lukou International Airport Highway have been reported to be 127 mg/L, 131 mg/L, 21.25 mg/L, 2.33 mg/L, 5.59 mg/L, and 0.37 mg/L, respectively [30], all of which surpass the standards for Class-III water quality under GB3838-2002. While samples have been collected under dry/wet [29] and variable rainfall conditions [30] in previous studies, we collected samples during the rainy season. Thus, our lower pollutant concentrations may be attributed to dilution [31]. Public pathways in the karst areas did not exhibit notably elevated concentrations of heavy metals, which may be attributed to the Ca-rich, slightly alkaline, and clay-rich karst soil [32] displaying strong heavy metal adsorption and fixation capacities [15, 16].

Chemical Composition of Highway Runoff

We delineated groundwater types based on our hydrochemical data using a Piper diagram, which aids in identifying groundwater sources, types, and hydrochemistry [33]. As shown in Fig. 3a), the cations at the YJ and BZJ sampling points predominantly consisted of Ca^{2+} (>80%). Meanwhile, at XC-1 and XC-4, Na^+ and K^+ accounted for 40–60% of all cations, and the predominant anion was HCO_3^- (80%). At XC-5, BZJ-1, and BZJ-4, Cl^- accounted for 30-40% (Fig. 3). Thus, we identified two hydrochemical types: Ca–HCO_3^- and (Ca–Na)–HCO_3^-. The sampling points were evenly distributed within the limestone-dominated formations, with XC-4 and XC-6 showing the highest total dissolved solids (TDS), possibly because of the widespread occurrence of Xincheng limestone (Fig. 1).

Gibbs diagrams [34] illustrate the relationship between TDS and both Na/(Na + Ca) and Cl/(Cl + HCO_3),

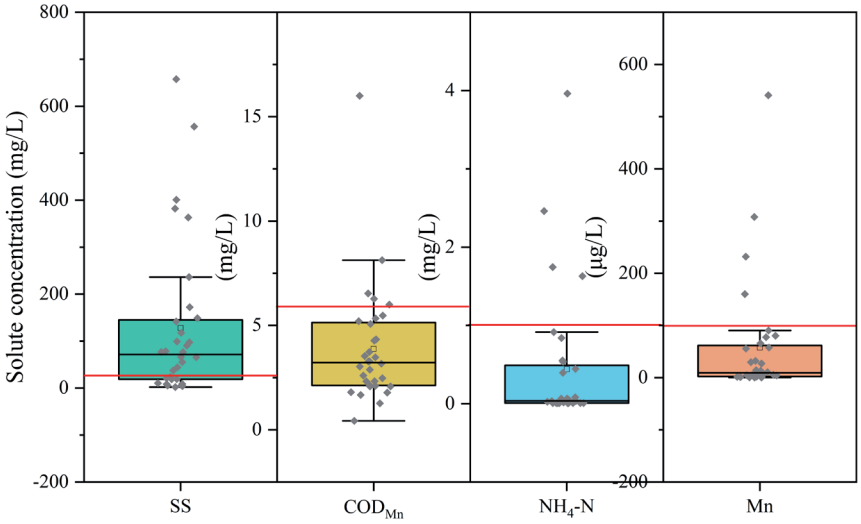

Fig. 2. Distribution of ions exceeding the Chinese government standards.
Note: Red lines represent the standard for Class-III water according to standard GB3838–2002.

allowing for the mechanisms governing groundwater hydrochemistry to be identified. By plotting measured data on a Gibbs diagram, precipitation, rock weathering, and evaporation were identified as key controls on groundwater hydrochemistry [33, 35]. Fig. 3b) (left) shows that most sampling points were plotted near the rock-weathering end-member, with only two points from BZJ plotting near precipitation. Fig. 3b) (right) also shows that most points from XC are plotted near precipitation. This suggests that groundwater recharge mainly originates from carbonate rock weathering, with precipitation also playing a key role. However, the Gibbs diagram could not account for anthropogenic inputs.

Solute Sources

In surface waters, K^+ and Na^+ typically originate from silicate weathering, atmospheric deposition, and anthropogenic activities [36], while Cl^- arises from salt dissolution, atmospheric deposition, and anthropogenic activities, and HCO_3^-, Ca^{2+}, and Mg^{2+} originate from carbonate weathering [37]. As there were no exposed evaporites in the watershed and the Gibbs diagram indicated a departure from the evaporite end-member, evaporite dissolution could be ignored. Previous studies have shown that rainfall is the primary source of Cl^- [38], the behavior of which is relatively stable in the surface water cycle. The concentrations of Cl^-, K^+, and

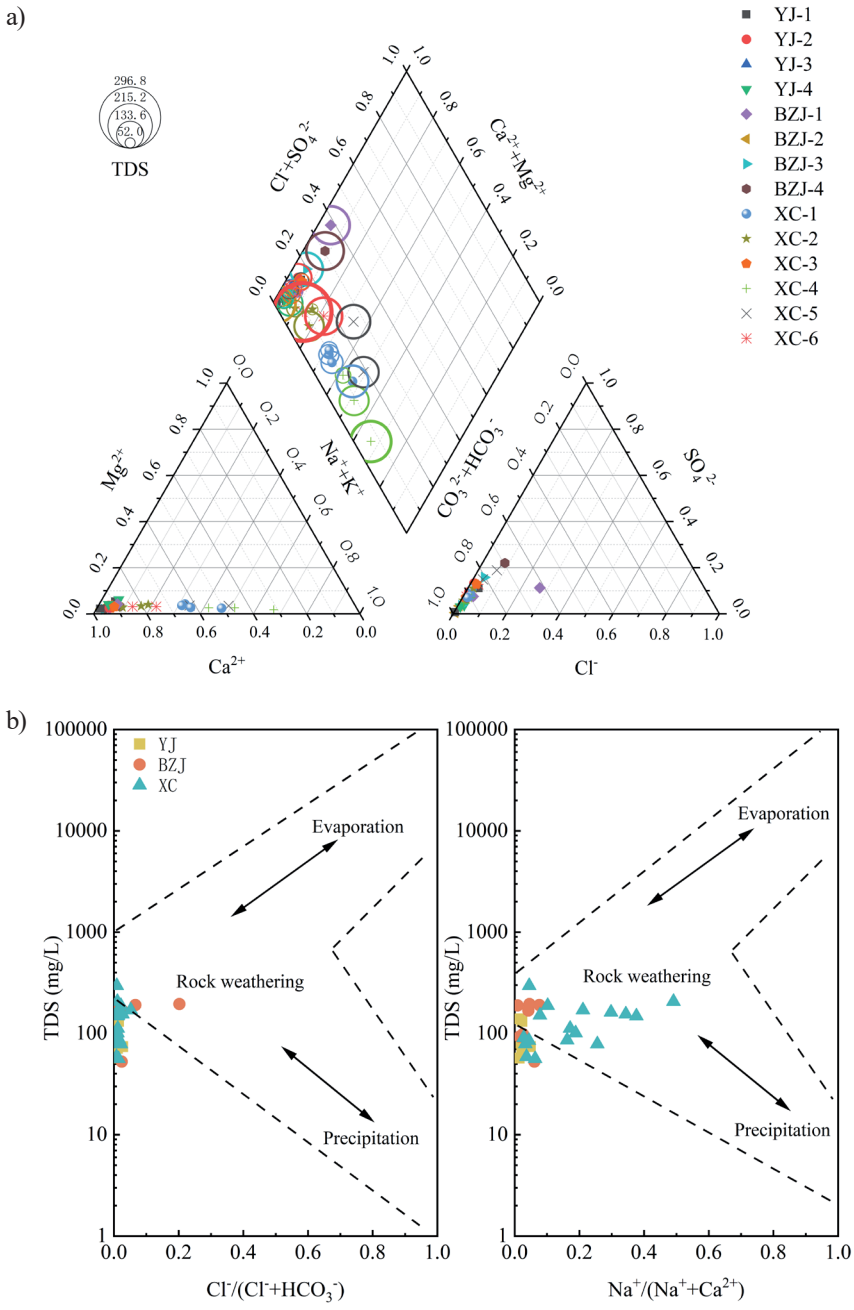

Fig. 3. Piper a) and Gibbs b) diagrams showing the hydrochemistry of the total dissolved solids (TDS) at the sampling points.

Na^+ in rainfall in Guilin City are 0.002–0.127 meq/L, 0.00–0.032 meq/L, and 0.00–0.17 meq/L, respectively [38]. In this study, runoff Cl^- concentrations fell within the range for rainfall, except for BZJ-1, BZJ-4, and XC-5, suggesting that Cl^- primarily originated from rainfall, with rainfall combined with anthropogenic activities making a smaller contribution. However, the K^+ and Na^+ concentrations exceeded the range for rainfall at most sites. The correlation among K^+, Na^+, and Cl^- was not significant, while that between K^+ and Na^+ was significant (Fig. 4), suggesting a common anthropogenic source of K^+ and Na^+.

The study area is affected by anthropogenic activities, including highway construction and traffic. NO_3^- predominantly stems from agriculture (e.g., fertilizers, atmospheric deposition, agricultural waste, excreta, and biomass burning) [39], while SO_4^{2-} largely originates from the dissolution of sulfide minerals, industrial and mining activities, and atmospheric acid deposition [36, 40]. Fig. 4 shows that the correlation between NO_3^- and SO_4^{2-} was not significant; however, both were significantly correlated with Cl^-, indicating that NO_3- and SO_4^{2-} also had mixed sources of rainfall and human activity, but their primary sources differed. To further analyze the sources of ions and heavy metals in the water, FA was conducted to identify the common factors among the main sources.

Factor Analysis

Factor Loading

In this study, R-type FA was used to acquire a Kaiser–Meyer–Olkin value of 0.576 (>0.50); a Bartlett sphericity test yielded $p = 0$ (<0.01), indicating that principal component analysis could be used to discern the sources of chemical components in runoff and their influencing factors. Using the FA function in SPSS v. 20, five principal factors (F1–F5) were extracted with eigenvalues > 1, cumulatively explaining 84.27% of the runoff chemistry.

Factor loading reveals the correlation between variables and common factors, with higher absolute values indicating greater representativeness [41], and Varimax rotation produces a clearer factor-loading matrix (Table 2). Extraction values indicate the degree to which each variable is explained by common factors and are typically considered satisfactory when >0.7 [42]. Table 2 shows that all components had extraction values near 0.7, indicating that F1–F5 represented the sources of each ion – F1 (Cu, Zn, Co, Mn, Ba, Ca^{2+}, SO_4^{2-}, and COD_{Mn}); F2 (Al, Cr, Ni, As, K^+, Na^+, Cl^-, and NO_3^-); F3 (Ca^{2+}, Sr, Mg^{2+}, HCO_3^-, and SS); and F5 (TP).

As shown in Table 1, COD_{Mn} exceeded Chinese national standards at BZJ, while Mn did so at YJ and BZJ, and both are closely associated with F1, indicating that traffic is a key source of COD_{Mn} and Mn. K^+ and Na^+ primarily originate from human activities and were observed at the highest concentrations in XC (Fig. 2). XC is only open to traffic in June, so construction (F2) is the main human activity. During highway construction, large amounts of exhaust and dust from vehicles, as well as sediment and soil, can enter runoff and water bodies through rainfall [2,43, 44].

F3 is closely linked to the weathering of carbonates, with Ca^{2+}, Mg^{2+}, and HCO_3^- being the common dissolution products. As a Ca^{2+}-homologue, Sr exhibits geochemical behaviors similar to those of Ca^{2+} and Mg^{2+} during carbonate dissolution [45]. In surface runoff, SS may originate from atmospheric deposition, tire wear, or road surface abrasion [2, 9, 10]. However, our SS extraction values exceeded those of Ca^{2+}, Mg^{2+},

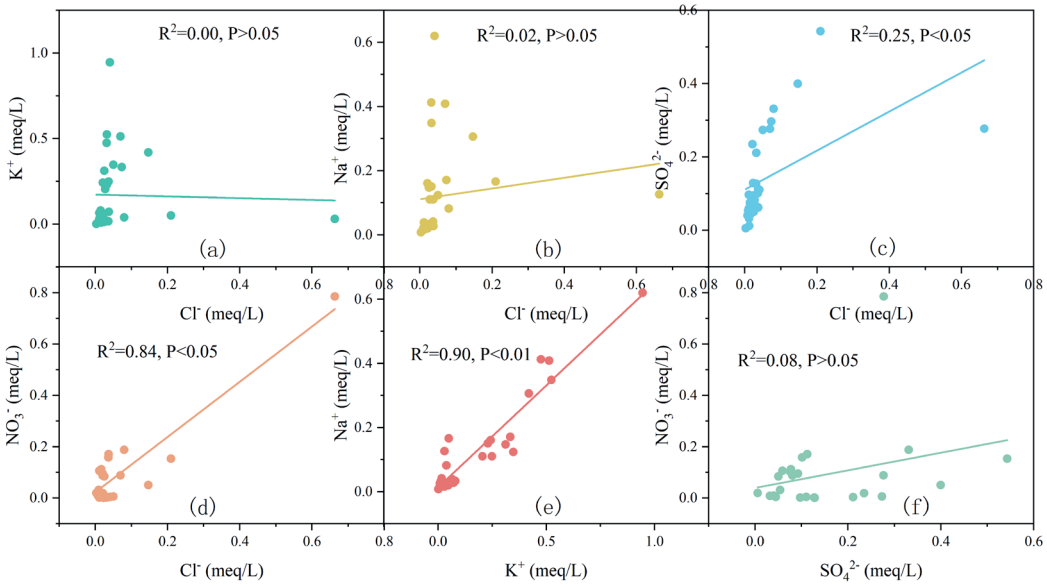

Fig. 4. Correlations between solutes in highway runoff.

Table 2. Rotational component matrix of factors.

Solute	Factor					Extraction
	1	2	3	4	5	
Cu	0.716					0.792
Zn	0.870					0.911
Co	0.901					0.953
Mn	0.935					0.898
Ba	0.875					0.897
Ca	0.524		0.675			0.940
SO_4^{2-}	0.613					0.781
COD_{Mn}	0.810					0.693
Al		0.798				0.696
Cr		0.913				0.865
Ni		0.767				0.894
As		0.844				0.730
K		0.757				0.811
Na		0.803				0.765
Sr			0.860			0.862
Mg			0.738			0.824
HCO_3^-			0.866			0.837
SS			0.888			0.811
Cl				0.911		0.962
NO_3^-				0.912		0.943
TP					0.906	0.831

Note: Extraction was performed via principal component analysis using the Varimax rotation method with Kaiser normalisation; rotation converged within five iterations.

and HCO_3^- for F3, indicating a strong association with the distribution of carbonates. In karst areas, soil erosion through surface and underground fissures is prevalent [46], and rainfall washes away and accumulates soil particles on road surfaces, potentially serving as the main cause of high SS concentrations. Thus, F3 represents the influence of carbonate geology on runoff chemistry.

Consistent with our correlation results, Cl^- and NO_3^- shared the same origin. Generally, NO_3^- and TP originate from fertilization along highways [2, 3]. However, NO_3^- was primarily influenced by F4, while TP was influenced by F5 (Table 2). Correlation analysis indicated that Cl^- largely originated from rainfall. Thus, F4 represents the combined effect of rainfall and artificial fertilization, while F5 represents the effect of fertilization alone.

Factor Scores

As F1–F3 explained 66% of the variance and represented the primary factors controlling runoff hydrochemistry, factor score analysis was performed for each sampling point to identify which was the main factor of influence at each site (Fig. 5). Each factor score plot is divided into four quadrants, with the upper right indicating that both factors control the major ion content and the lower right and upper left quadrants indicating that ion content is controlled by the horizontal and vertical axis factors, respectively. The lower left quadrant suggests that ion contents were influenced to a lesser extent by both axes.

Fig. 5a) shows that the sampling points in YJ and BZJ were mainly located in the lower right quadrant, indicating that they were primarily influenced by F1. Most XC samples were distributed in the upper left quadrant, indicating that F2 was the primary factor controlling runoff hydrochemistry; however, some XC samples were controlled by F3 (Fig. 5b), and others were jointly influenced by F2 and F3 (Fig. 5c). Meanwhile, YJ and BZJ were jointly controlled by F1 and F3 (Fig. 5b) and less influenced by F2 (Fig. 5c). Overall, YJ and BZJ were primarily controlled by F1 (highway traffic) and F3

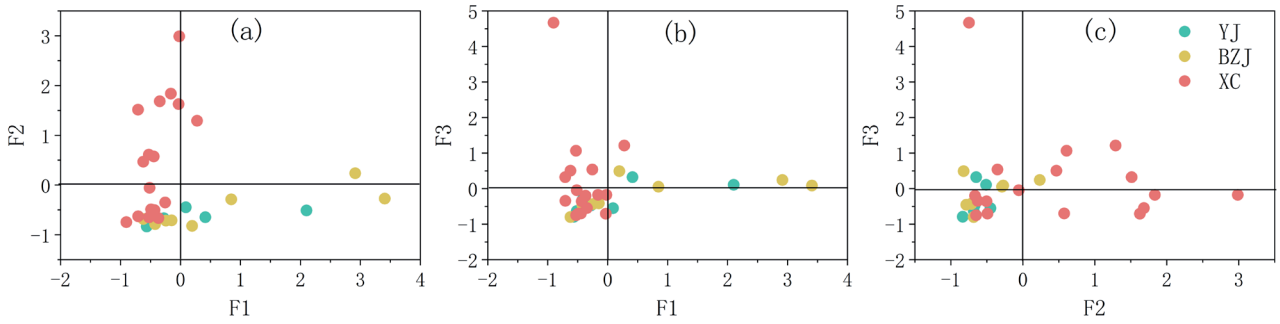

Fig. 5. The first three factor scores (F1–F3) for the sampling sites.
Note: F1, traffic; F2, construction; F3, carbonate weathering.

(carbonate weathering), consistent with their 15 years of operation and geological background. XC is jointly controlled by F2 (highway construction) and F3, which corresponds to the construction of the highway during the sampling period and the widespread distribution of the carbonates. These findings support the accuracy of factor analysis.

Effects of Karst Carbon Sequestration on Highway Runoff

Ca^{2+} and HCO_3^- primarily originate from carbonate weathering but can also result from soil leaching and rainfall [47]. In this study, the Ca^{2+} concentration in BZJ was the highest, followed by those in YJ and XC, while the mean and range of Mg^{2+} were relatively consistent among the three locations. The HCO_3^- concentration was also highest in BZJ, followed by XC and YJ. A comparison of these three ions with the concentrations and carbon sink values of epikarst springs YJ-S31 and BDP in the Guilin area reveals that the Ca^{2+} and HCO_3^- concentrations were 20–100 times higher than those in the rainwater and 20–25% of those in the surface springs (Table 3, Fig. 6). However, it appears that the concentrations of Ca^{2+} and HCO_3^- from rainfall and soil leaching did not exceed those in the surface streams of the Guilin area (XLB, Table 3), though the concentrations of Ca^{2+} and HCO_3^- at all three sampling points were 3–4 times higher than those in the XLB [20], indicating that the excess was derived from carbonate weathering. This suggests that when rainwater is collected as runoff on the surface, embankments, slopes, or medians of highways, it has been influenced by carbonate weathering and thus acts as a carbon sink. The Mg^{2+} concentration in the BDP was 20 times higher than that at the study points, which was attributed to the fact that the bedrock of the BDP consists of dolomite with a higher magnesium content [20].

The sampling period for YJ and BZJ spanned from April–May, while that for XC ranged from April–July. The daily CCSFs for YJ, BZJ, and XC are shown in Table 3. The carbon sequestration capacity of runoff in YJ and BZJ amounted to 15–21% of that of epikarst springs in the same region (i.e., YJ-S31 and BDP) [20, 48], representing a 3.44–4.64-fold increase compared to silicate basins (XLB) [20]. The proportion may experience minor fluctuations attributable to interannual variations in rainfall, according to eq. (2). XC exhibited a higher capacity due to higher precipitation, where the runoff volume emerged as the primary determinant [49], even under conditions of HCO_3^- content approximating that of BZJ. Highways in karst regions play a pivotal role

Table 3. Carbonate carbon-sink fluxes (CCSFs) among highway runoff, karst spring, and surface water samples in Guangxi.

Sample Site	Ca^{2+} mg/L	Mg^{2+} mg/L	HCO_3^- mg/L	CCSF kg C/km^{2}d
YJ	21.11	0.54	65.37	9.07
BZJ	33.82	0.55	85.65	12.26
XC	20.98	0.58	85.15	35.71
YJ S31	90.95	0.60	284	57.54 [48]
BDP	95.33	11.70	304.75	46.09 [20]
XLB	7.00	1.76	18.3	2.64 [20]
Rainfall	4.00	0.52	4.5	/

Abbreviations: BDP, epikarst spring in the Guilin area; BZJ, adjacent to the Baizhujing Reservoir; XC, the Laidu Expressway in Xincheng County; XLB, surface streams in the Guilin area; YJ, Yaji section of the Guilin Ring Expressway; YJ S31, epikarst spring near YJ.

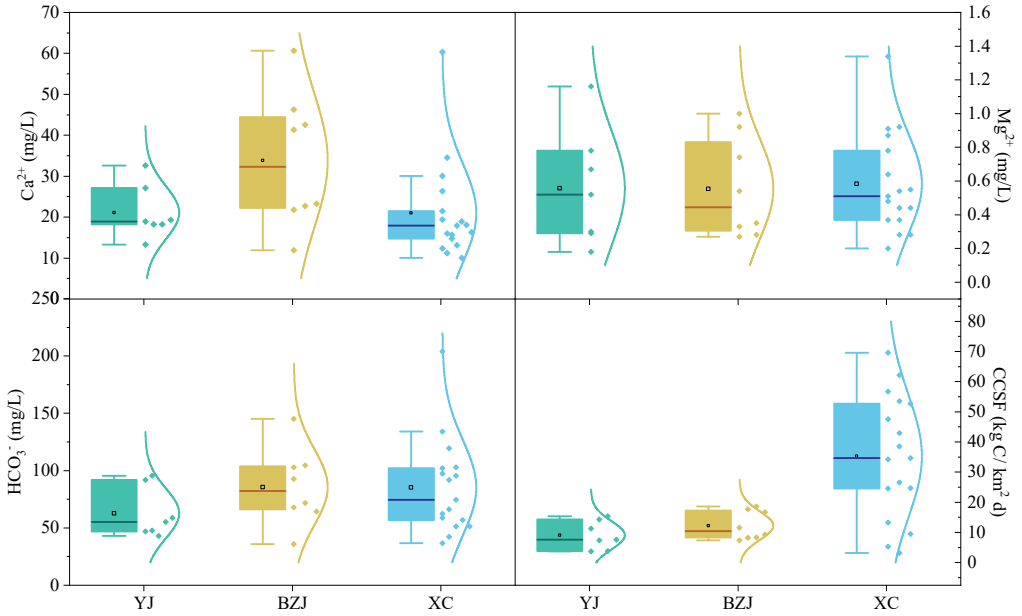

Fig. 6. Concentrations of major ions and carbon sink in highway runoff.

in carbon sequestration, highlighting their importance for ecological restoration and energy conservation.

We exclusively sampled during the rainy season, which may have resulted in lower pollutant concentrations than the annual mean due to dilution. As carbon sequestration capacity remains elevated year-round, the proportions of CCSFs across different months in the same region may be miscalculated. Future research should involve intensified sampling during individual rainfall events to acquire EMCs and elucidate pollutant flushing patterns, thereby providing support for pollution remediation strategies for karstic highway runoff.

Conclusions

Our results provide insights into the pollution status and sources, and carbon sequestration of highway runoff in the karst areas of Guangxi. We identified SS, COD_{Mn}, NH_3–N, and Mn as the primary pollutants. FA revealed five main pollutant sources: traffic (F1), construction (F2), carbonate weathering (F3), rainfall combined with artificial fertilizer (F4), and artificial fertilizers alone (F5). Traffic (F1) and carbonate weathering (F3) emerged as the dominant factors at YJ and BZJ, while F3 and F2 were the main factors in XC. The carbon sequestration capacities of runoff in the YJ, BZJ, and XC areas were 9.07, 12.26, and 35.71 kg • C/km^2 d. YJ and BZJ accounted for 15-21% of that observed in a karst spring in the same region – a 3.44-34.64 – fold increase compared to silicate basins. These findings should inform the development of strategies for controlling pollution and carbon sequestration in karstic highway runoff. Further research is needed to explore pollutant flushing patterns and validate carbon capacities across seasons and locations.

Acknowledgments

This study was funded by National Natural Science Foundation of China (grant no.42277077), Natural Science Foundation of Guangxi [grant nos. 2022GXNSFAA035569, 2021GXNSFBA220065], the Project of the China Geological Survey [grant no. DD20230547], the Key Science and Technology Projects in the Guangxi Transport Industry [grant no. GXHS-2022-016], the Guilin Science Research and Technology Development Plan Project [grant no. 2020010905] and the Natural Resources Science and Technology Strategic Research Project [grant no. 2023-ZL-23]. We would like to thank Editage (www.editage.cn) for English language editing.

Conflict of Interest

The authors declare no conflict of interest.

References

1. JIA Z., WANG J., ZHOU X., ZHOU Y., LI Y., LI B., ZHOU S. Identification of the sources and influencing factors of potentially toxic elements accumulation in the soil from a typical karst region in Guangxi, Southwest China. Environmental Pollution, **256**, 113505, **2020**.
2. MÜLLER A., ÖSTERLUND H., MARSALEK J., VIKLANDER M. The pollution conveyed by urban runoff:

A review of sources. Science of the Total Environment, **709**, 136125, **2020**.
3. HUBER M., WELKER A., HELMREICH B. Critical review of heavy metal pollution of traffic area runoff: Occurrence, influencing factors, and partitioning. Science of the Total Environment, **541**, 895, **2016**.
4. CHARTERS F.J., COCHRANE T.A., O'SULLIVAN A.D. The influence of urban surface type and characteristics on runoff water quality. Science of The Total Environment, **755**, 142470, **2021**.
5. THORPE A., HARRISON R.M. Sources and properties of non-exhaust particulate matter from road traffic: A review. Science of the Total Environment, **400** (1-3), 270, **2008**.
6. PETRUCCI G., GROMAIRE M.C., SHORSHANI M.F., CHEBBO G. Nonpoint source pollution of urban stormwater runoff: a methodology for source analysis. Environmental Science and Pollution Research, **21** (17), 10225, **2014**.
7. OMRANI M., RUBAN V., RUBAN G., LAMPREA K. Assessment of atmospheric trace metal deposition in urban environments using direct and indirect measurement methodology and contributions from wet and dry depositions. Atmospheric Environment, **168**, 101, **2017**.
8. KAYHANIAN M. Trend and concentrations of legacy lead (Pb) in highway runoff. Environmental Pollution. **160**, 169, **2012**.
9. MARKIEWICZ A., BJÖRKLUND K., ERIKSSON E., KALMYKOVA Y., STRÖMVALL A.M., SIOPI A. Emissions of organic pollutants from traffic and roads: Priority pollutants selection and substance flow analysis. Science of the Total Environment, **580**, 1162, **2017**.
10. HORTON A.A., WALTON A., SPURGEON D.J., LAHIVE E., SVENDSEN C. Microplastics in freshwater and terrestrial environments: Evaluating the current understanding to identify the knowledge gaps and future research priorities. Science of the Total Environment, **586**, 127, **2017**.
11. DE SILVA S., BALL A.S., HUYNH T., REICHMAN S.M. Metal accumulation in roadside soil in Melbourne, Australia: Effect of road age, traffic density and vehicular speed. Environmental Pollution, **208**, 102, **2016**.
12. MURPHY L.U., COCHRANE T.A., O'SULLIVAN A. Build-up and wash-off dynamics of atmospherically derived Cu, Pb, Zn and TSS in stormwater runoff as a function of meteorological characteristics. Science of the Total Environment, **508**, 206, **2015**.
13. PERERA T., MCGREE J., EGODAWATTA P., JINADASA K., GOONETILLEKE A. New conceptualisation of first flush phenomena in urban catchments. Journal of Environmental Management, **281**, 111820, **2021**.
14. BAKR A.R., FU G.Y., HEDEEN D. Water quality impacts of bridge stormwater runoff from scupper drains on receiving waters: A review. Science of the Total Environment, **726**, 138068, **2020**.
15. HUANG F., WEI X., ZHU T., LUO Z., CAO J. Insights into Distribution of Soil Available Heavy Metals in Karst Area and Its Influencing Factors in Guilin, Southwest China. Forests, **12** (5), 609, **2021**.
16. WEN Y., LI W., YANG Z., ZHUO X., JI J. Evaluation of various approaches to predict cadmium bioavailability to rice grown in soils with high geochemical background in the karst region, Southwestern China. Environmental Pollution, **258**, 113645, **2020**.
17. CAO J., WU X., HUANG F., HU B., GROVES C., YANG H., ZHANG C. Global significance of the carbon cycle in the karst dynamic system: evidence from geological and ecological processes. China Geology, 17, **2018**.
18. SUN P., HE S., YU S., PU J., YUAN Y., ZHANG C. Dynamics in riverine inorganic and organic carbon based on carbonate weathering coupled with aquatic photosynthesis in a karst catchment, Southwest China. Water Research, **189**, 116658, **2021**.
19. SUN P.A., XIAO Q., GUO Y., MIAO Y., WANG Q., CHENG Z. Carbonate dissolution rate and karst carbon sink in mixed carbonate and silicate terrain: Take the upper reaches of the Lijiang River basin as an example. Carsologica Sinica, **40** (5), 825, **2021** [in Chinese].
20. HUANG F., ZHANG C.L., XIE Y.C., LI L., CAO J.H. Inorganic carbon flux and its source in the karst catchment of Maocun, Guilin, China. Environmental Earth Sciences, **74** (2), 1079, **2015**.
21. DING M., WU X., CAO J., HU X., PAN M., HUANG F., REN M. Characteristics and influencing factors of vertical carbon migration in the cave system of Liangfeng cave in Guilin. Carsologica Sinica, **40** (4), 600, **2021** [in Chinese].
22. CEN H., QIU R., YANG P. Discussion on Soil Buffering Mechanisms of Acid Precipitation. Research of Environmental Sciences, **13** (2), 49, **2000**.
23. KIM J.H., JOBBÁGY E.G., RICHTER D.D., TRUMBORE S.E., JACKSON R.B. Agricultural acceleration of soil carbonate weathering. Global Change Biology, **26** (10), 5988, **2020**.
24. WANG F., LAI H.X., LI Y.B., FENG K., TIAN Q.Q., GUO W.X., QU Y.P., YANG H.B. Spatio-temporal evolution and teleconnection factor analysis of groundwater drought based on the GRACE mascon model in the Yellow River Basin. Journal of Hydrology, **626**, **2023**.
25. ZENG S., LIU Z., KAUFMANN G. Sensitivity of the global carbonate weathering carbon-sink flux to climate and land-use changes. Nature Communications, **10** (1), 5749, **2019**.
26. The Ministry of Environmental Protection of the People's Republic of China. Environmental quality standards for surface water, GB3838-2002, **2002**.
27. General Administration of Quality Supervision, Inspection and Quarantine of the People's Republic of China. The reuse of urban recycling water – Water quality standard for scenic environment use, GB/T 18921-2019, **2019** [In Chinese].
28. SMITH K.P., SORENSON J.R., GRANATO G.E. Characterization of stormwater runoff from bridge decks in eastern Massachusetts, 2014-16. US Geological Survey, **2018**.
29. LI Q. Research on Pollution Characteristics and Treatment Countermeasures of Runoff Based on Liuzhen Express in Guizhou Province. Beijing, **2018** [in Chinese].
30. LI H., ZHANG X., GAO H., FU D. Characterization of contaminated runoff on free way surface. China Environmental Science, **28** (11), 1037, **2008** [In Chinese].
31. WESTERLUND C., VIKLANDER M., BÄCKSTRÖM M. Seasonal variations in road runoff quality in Lulea, Sweden. Water Science and Technology, **48** (9), 93, **2003**.
32. ZHU T., ZENG S., QIN H., ZHOU K., YANG H., LAN F., HUANG F., CAO J., MÜLLER C. Low nitrate retention capacity in calcareous soil under woodland in the karst region of southwestern China. Soil Biology & Biochemistry, **97**, 99, **2016**.
33. REDWAN M., MONEIM A.A.A. Factors controlling groundwater hydrogeochemistry in the area west of Tahta, Sohag, Upper Egypt. Journal of African Earth Sciences, **118**, 328, **2016**.

34. GIBBS R.J. Mechanisms Controlling World Water Chemistry. Science, **170** (3962), 1088, **1970**.
35. XIAO J., JIN Z.D., WANG J., ZHANG F. Hydrochemical characteristics, controlling factors and solute sources of groundwater within the Tarim River Basin in the extreme arid region, NW Tibetan Plateau. Quaternary International, **380**, 237, **2015**.
36. GONG X.Y., WENG B.S., YAN D.H., YANG Y.H., YAN D.M., NIU Y.Z., WANG H. Potential recharge sources and origin of solutes in groundwater in the central Qinghai-Tibet Plateau using hydrochemistry and isotopic data. Journal of Hydrology-Regional Studies, **40**, **2022**.
37. LI Z.J., LI Z.X., FAN X.J., WANG Y., SONG L.L., GUI J., XUE J., ZHANG B.J., GAO W. D. Transformation mechanism of ions on different waters in alpine region. Chemosphere, **248**, **2020**.
38. ZHU H., LI Y., WU L., YU S., XIN C., SUN P., XIAO Q., ZHAO H., ZHANG Y., QIN T. Impact of the atmospheric deposition of major acid rain components, especially NH_4, on carbonate weathering during recharge in typical karst areas of the Lijiang River basin, southwest China. Applied Geochemistry, **114**, 104518, **2020**.
39. TAO L.C., CUN D.X., TU C.L., MA Y.Q., LIU Z.N., YIN L.H., HE C.Z., PANG L., ZHANG Q.D. Hydrochemical Characteristics and Control Factors of Surface Water in Kuaize River Basin at the Upper Pearl River. Environmental Science, **44** (11), 6025, **2023**.
40. HAN G.L., LIU C.Q. Water geochemistry controlled by carbonate dissolution: a study of the river waters draining karst-dominated terrain, Guizhou Province, China. Chemical Geology, **204** (1-2), 1, **2004**.
41. LI Z.X., QI F., WANG Q.J., SONG Y., LI H.Y., LI Y.G. The influence from the shrinking cryosphere and strengthening evopotranspiration on hydrologic process in a cold basin, Qilian Mountains. Global and Planetary Change, **144**, 119, **2016**.
42. LI Z.J., SONG L.L., MA J.Z. Hydrochemical characteristics and environmental significance in different ablation period in Hulugou River Basin in Qilian Mountain. Environmental Earth Sciences, **76** (17), **2017**.
43. MARSALEK J. Urban water cycle processes and interactions: urban water series-UNESCO-IHP. CRC press, **2014**.
44. SAJJAD R.U., PAULE-MERCADO M.C., SALIM I., MEMON S., SUKHBAATAR C., LEE C.H. Temporal variability of suspended solids in construction runoff and evaluation of time-paced sampling strategies. Environmental Monitoring and Assessment, **191** (2), **2019**.
45. SU C., YANG Y., BA J., LUO F., LI X., ZHAO G. Dynamic characteristics and genesis of strontium-rich groundwater in Xintian county, Hunan Province. Carsologica Sinica, **39**, (1), 24, **2020** [in Chinese].
46. PENG X.D., DAI Q.H., LI C.L., XU S.B. The underground leakage process of soil patches around bedrock outcrops in a karst rocky desertification area traced using rare earth elements. Journal of Hydrology, **619**, **2023**.
47. HUANG C.Y. Soil Science. China Argiculture Press, Beijing, **2000**.
48. XIN C. Characteristics of karst hydrochemistry and carbon sink at Yaji test site, Guilin. Northwest Normal University, Lanzhou, **2023** [in Chinese].
49. KANG Z., CHEN J., YUAN D., HE S., LI Y., CHANG Y., DENG Y., CHEN Y., LIU Y., JIANG G., WANG X., ZHANG Q. Promotion function of forest vegetation on the water & carbon coupling cycle in karst critical zone: Insights from karst groundwater systems in south China. Journal of Hydrology, **590**, 125246, **2020**.